

Review

Oxygen Reduction Reaction Catalyzed by Noble Metal Clusters

Zhenghua Tang ^{1,2,*} , Wen Wu ¹ and Kai Wang ¹

¹ Guangzhou Key Laboratory for Surface Chemistry of Energy Materials, New Energy Research Institute, School of Environment and Energy, South China University of Technology, Guangzhou Higher Education Mega Centre, Guangzhou 510006, China; wuwen0730@163.com (W.W.); wangkai163x@126.com (K.W.)

² Guangdong Provincial Key Laboratory of Atmospheric Environment and Pollution Control, Guangdong Provincial Engineering and Technology Research Center for Environmental Risk Prevention and Emergency Disposal, South China University of Technology, Guangzhou Higher Education Mega Centre, Guangzhou 510006, China

* Correspondence: zhht@scut.edu.cn

Received: 2 January 2018; Accepted: 2 February 2018; Published: 7 February 2018

Abstract: Highly-efficient catalysts for the oxygen reduction reaction (ORR) have been extensively investigated for the development of proton exchange membrane fuel cells (PEMFCs). The state-of-the-art Pt/C catalysts suffer from high price, limited accessibility of Pt, sluggish reaction kinetics, as well as undesirable long-term durability. Engineering ultra-small noble metal clusters with high surface-to-volume ratios and robust stabilities for ORR represents a new avenue. After a simple introduction regarding the significance of ORR and the recent development of noble metal clusters, the general ORR mechanism in both acidic and basic media is firstly discussed. Subsequently, we will summarize the recent efforts employing Pt, Au, Ag, Pd and Ru clusters, as well as the alloyed bi-metallic clusters for acquiring highly efficient catalysts to enhance both the activity and stability of ORR. Molecular noble metal clusters with definitive composition to reveal the relevant ORR mechanism will be particularly highlighted. Finally, the current challenges, the future outlook, as well as the perspectives in this booming field will be proposed, featuring the great opportunities and potentials to engineering noble metal clusters as highly-efficient and durable cathodic catalysts for fuel cell applications.

Keywords: noble metal clusters; oxygen reduction reaction; single metal clusters; alloyed bimetallic clusters; fuel cells

1. Introduction

With a variety of merits including high energy density, excellent portability and low operation temperature, proton exchange membrane fuel cells (PEMFCs) hold great promises as commercially-viable electric power sources toward various applications, especially for automotive vehicles [1,2]. To achieve the large-scale commercialization of PEMFCs, the biggest challenge arises from the sluggish oxygen reduction reaction occurring at the cathode [3–6]. The current state-of-the-art electrocatalyst for the oxygen reduction reaction (ORR) is Pt nanoparticles (5–10 nm in diameter) dispersed in porous carbon materials (denoted as Pt/C) [7–10]. Even if Pt is considered as the best choice as the catalyst, there are several significant limitation factors that hinder its widespread utilizations [11,12]. First of all, the scant availability of Pt and resulting high price comprise one of the major drawbacks of such a catalyst. Note that the price of the Pt/C catalyst accounts for 50% of the cost of a fuel-cell stack [13]. Secondly, such a Pt/C catalyst still suffers from slow reaction kinetics, resulting in undesirable performance [14]. The final challenging problem comes from the technical issue regarding the poor long-term stability of Pt under operational conditions. The Pt/C catalyst is

susceptible to dissolution, sintering and agglomeration, resulting in loss of performance [15]. Note that, Pt-based catalysts exhibited a poor tolerance to methanol, hence generating CO, leading to the blocking of Pt active sites and diminishing of catalytic activity.

Noble metal clusters, also named monolayer protected clusters (MPCs), include a metal core and surrounding protecting ligands, which can be phosphine molecules, thiolate organic nonmetallic compounds, polymers, as well as biological macromolecules [16–18]. MPCs normally consist of about ten to a few hundred atoms, with an ultrasmall size usually less than 2 nm in diameter. As a special class of nanomaterials, MPCs show strong quantum confinement effects due to their ultrasmall size. For instance, Au MPCs exhibited size-dependent optical and electrochemical properties [19], which are quite different from their counterparts of Au nanoparticles with relatively larger dimensions. Particularly, with kinetic control or rationally-designed synthetic methodologies, MPCs with molecular purity of atomic precision can be acquired, as a definitive formula of M_xL_y , where M, L denote metal and ligand while x and y are the number of atoms, respectively. Molecule-like characteristics and physicochemical properties can be observed for these molecular noble metal clusters. A perfect example is molecular Au clusters, as manifested by the discrete energy levels of electrons, multiple absorbance bands, enhanced photoluminescence, non-linear optical behaviors and other characteristic physiochemical properties.

Regarding the fabrication of the noble metal clusters, seminal work was done by Brust et al. [20,21]. Through the biphasic synthetic approach, polydisperse Au nanoclusters with a size ranging from 1–5 nm were acquired. Note that most bimetallic clusters are still fabricated by this wet-chemical strategy. As the Brust method cannot achieve atomic precision and molecular purity, post-synthetic purification such as electrophoretic isolation coupled with mass spectrometry has been conducted to obtain molecular Au clusters, such as $Au_{15}(SG)_{13}$ (SG-glutathione thiolate), $Au_{18}(SG)_{14}$, $Au_{22}(SG)_{16}$, $Au_{22}(SG)_{17}$, $Au_{25}(SG)_{18}$, $Au_{29}(SG)_{20}$, $Au_{33}(SG)_{22}$ and $Au_{39}(SG)_{24}$ [22,23]. To achieve molecular Au clusters during the synthesis, one effective strategy is the kinetic control approach, in which the reaction conditions including temperature, reaction rate and other parameters are optimized. A perfect example is $Au_{25}(SC_2H_4Ph)_{18}$, and the kinetic control approach developed by Jin's group can offer ultra-high purity with high yield [24]. Besides that, ligand-induced etching or annealing has also been extensively employed. Qian et al. reported the synthesis of molecular $Au_{38}(SC_2H_4Ph)_{24}$ clusters, in which polydisperse Au clusters protected by glutathione were first made, and subsequently, the size-mixed Au_n clusters reacted with excess PhC_2H_4SH for ~40 h at 80 °C, leading to $Au_{38}(SC_2H_4Ph)_{24}$ clusters of molecular purity [25]. In the past decade, with the efforts from multiple research groups, a series of molecular Au clusters including Au_4 [26], Au_{11} [27], Au_{18} [28,29], Au_{25} [30], Au_{38} [25], Au_{55} [31], Au_{102} [32], Au_{130} [33] and Au_{144} [34] molecules with atomic precision has been successfully achieved by the kinetic control approach, size-focusing strategy and ligand-induced transformation. We have also witnessed the successful crystallization of several molecular Au clusters, such as $Au_{11}(PPh_3)_7Cl_3$ (PPh_3 -Triphenylphosphine) and $Au_{11}(PPh_3)_8Cl_3$ [27], $Au_{18}(SR)_{14}$ (where R = CH_3 , C_6H_5 , C_6H_{11}) [28,29], $Au_{25}(SC_2H_4Ph)_{18}$ [35,36], $Au_{38}(SC_2H_4Ph)_{24}$ [37], $Au_{102}(p\text{-MBA})_{40}$ [38] ($p\text{-MBA}$ = *para*-mercaptobenzoic acid), and so on.

Enhanced and unusual catalytic performance can be also achieved for the noble metal clusters regardless of the sample dispersity. Notably, the emergence and rapid development of noble metal clusters provide great opportunities to potentially resolve the activity and durability issues for ORR in the electrocatalytic process. First of all, the ORR activity highly relies on the catalytic active sites of the exposed surface, and the high-surface-to-volume ratio, as well as ultra-small dimension impart MPCs with unique advantages. Secondly, with the surface capping agents as the ligand or stabilizer, MPCs can resist agglomeration, sintering and decomposition, and the resulting robust stability is favorable for long-term cycling of the potential scan during the electrocatalytic process.

This review mainly focuses on the recent progresses regarding employing noble metal clusters as high-efficiency catalysts for ORR. The general mechanism regarding ORR in acid media and alkaline solution will be firstly discussed. Then, we will provide a comprehensive overview of current efforts

by using noble metal clusters especially Pt, Au, Ag, Pd, Ru and alloyed bi-metallic clusters for ORR toward fuel cell applications. The review will be concluded with the summarized current challenges and the outlook for the further research directions.

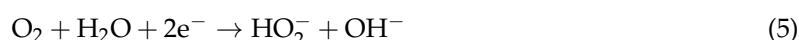
2. The General ORR Mechanism

In acidic electrolyte or basic electrolyte, different mechanisms have been well documented for ORR [3,6,39]. However, multiple electron transfer occurs in the ORR process regardless of the electrolyte. Such a process can be illustrated by the following equations [40]:

In acidic electrolytes:



In alkaline electrolytes:



It can be observed that, in either electrolyte, two possible pathways can be adopted for ORR. One is the direct 4e^- reduction to form H_2O in acid solution or OH^- in basic solution, while in the other pathway, a 2e^- reduction occurs to generate H_2O_2 or HO_2^- first, followed by the sequent further reduction to H_2O or OH^- with another 2e^- transfer.

A direct 4e^- pathway is usually favorable for Pt-based catalysts especially the benchmark commercial Pt/C catalyst in both electrolytes, but the intrinsic ORR process on a Pt surface is complicated and not well understood [41]. For the four-electron process, there are two possible pathways (dissociative and associative mechanisms) in both media solutions [41]. The related mechanisms in alkaline solution are illustrated as follows:

Dissociative mechanism:



where $*$ denotes the catalytic active site on a certain surface. In this mechanism, O_2 is adsorbed firstly, then the O–O bond is cleaved to form two adsorbed atomic O^* species. The O^* species further gains two protons and two electrons to form OH^* and eventually forms OH^- by gaining two electrons.

Associative mechanism: For the associative mechanism, there are two possible pathways (4e^- or 2e^-) involved as follows:

The 4e^- pathway:



or the 2e^- pathway:





Whether the reaction takes a dissociative or an associative pathway mainly depends on the initial O_2 dissociating energy barrier on a provided surface [42]. Previous first-principle calculations have shown that the adsorbed oxygen species including OOH^* , OH^* and HOOH^* might be involved during the ORR process [43]. For other noble metal nanoparticle- or nanocluster-based catalysts, either the direct 4e^- pathway or the $2\text{e}^- + 2\text{e}^-$ pathway has been extensively reported, depending on the physicochemical properties of the catalyst [14,39].

Furthermore, the binding affinity to the oxygenated species plays an important role in determining the ORR catalytic activity. The volcano-shaped relationship between the ORR activity and the OOH^* , OH^* and HOOH^* binding energy have been recognized on a great deal of metal surfaces [44,45]. Such variation of the binding energy to the oxygenated species from different metal surfaces is actually highly dependent on the electronic structure of the catalyst. The optimal electronic structure with appropriate binding energy of the intermediates will eventually lead to optimized catalytic performance for ORR.

3. Engineered Noble Metal Clusters for ORR

The ORR performance of all the noble metal clusters mentioned in this review is summarized in Table 1. The size of these metal clusters, the electrolyte employed in ORR, the ORR activity parameter such as onset potential, half-wave potential, diffusion-limited current density at specific rotating rate, as well as the corresponding reference are included. Subsequently, we will discuss the details regarding ORR catalyzed by single noble metal clusters (Pt clusters, Au clusters, Ag clusters, Pd and Ru clusters) and alloyed bimetallic clusters, separately.

Table 1. The ORR performance summary catalyzed by noble metal clusters listed in this review. The catalyst, electrolyte, onset potential, half-wave potential, diffusion-limited current density, rotating rate, number of electron transfer, size and corresponding reference are included.

| | Catalysts | Electrolyte | E_{onset} (V vs. RHE) | $E_{1/2}$ (V vs. RHE) | j (mA cm $^{-2}$) | Rotating Rate (rpm) | n | Size (nm) | Reference |
|--------------------|------------------------------------|--------------------------------------|----------------------------|--------------------------|----------------------|---------------------|-----------|------------|-----------|
| Pt clusters | Pt ₁₂ @3 | 0.5 M H ₂ SO ₄ | 0.72 | / | 1.28 | 300 | / | 0.9 ± 0.1 | [46] |
| | G6-OH (Pt ₂₄₀) | 0.1 M HClO ₄ | 0.95 | 0.82 | 4.5 | 900 | / | 1.9 ± 0.29 | [47] |
| | Pt ₁₄₇ DENs | 0.1 M HClO ₄ | 0.9 | / | / | / | 3.7 | 1–2 | [48] |
| | (Pt-3Sn) complex | 0.1 M HClO ₄ | 0.98 | / | / | / | / | / | [49] |
| | Pt-GC | 0.1 M HClO ₄ | 0.98 | 0.82 | 7.6 | / | / | 1.5 | [50] |
| | Pt-C (Mo ₂ C) 800 °C | 0.5 M H ₂ SO ₄ | 0.98 | 0.83 | 6.5 | 3000 | 3.6 ± 0.1 | / | [51,52] |
| | Pt-on-Pd/C | 0.1 M HClO ₄ | 0.99 | 0.862 | 5.9 | / | / | 1–2 | [53] |
| Au clusters | Pt/FeCo-OMPC (L) | 0.1 M HClO ₄ | 0.98 | 0.85 | 5.6 | / | / | 2–3 | [54] |
| | Au ₁₁ /GC | 0.1 M KOH | 0.87 | / | 7 | 1600 | 3.9 | 0.8–1.7 | [55] |
| | Au/Pt/C | 0.1 M HClO ₄ | 0.98 | 0.84 | 6 | 1600 | / | 3 | [56] |
| | Au 3 nm cluster | 0.5 M KOH | 0.84 | / | 8.2 | 2500 | 4 | 3 | [57] |
| | Au/rGO | 0.1 M KOH | 0.87 | / | 4 | 1600 | 3.7–3.9 | 1.8 ± 0.2 | [58] |
| | s-Graphene/PyPBI/Au _{1.6} | 0.1 M KOH | 0.87 | 0.72 | 3 | 1600 | / | 1.6 ± 0.3 | [59] |

Table 1. Cont.

| Catalysts | Electrolyte | E_{onset} (V vs. RHE) | $E_{1/2}$ (V vs. RHE) | j (mA cm ⁻²) | Rotating Rate (rpm) | n | Size (nm) | Reference | |
|-----------------------------|--|----------------------------|--------------------------|----------------------------|------------------------|-----------|-------------|-----------|------|
| BOD-AuNC/ SWNT | 0.1 M phosphate buffer (pH = 7.5) | 1.17 | 1.07 | / | 1600 | / | 0.9 | [60] | |
| AuNCs: RGO = 1:1 | 0.1 M KOH | 0.7 | / | 3 | 2500 | / | 2.4 ± 0.7 | [61] | |
| AuCNs-30% | 0.1 M KOH | 0.96 | 0.84 | 4 | 2500 | 3.5–3.86 | 2.59 ± 0.7 | [62] | |
| AuPC-1 | 0.1 M KOH | 0.95 | 0.83 | 3.9 | 2500 | 3.6–3.92 | 3.7 ± 0.9 | [63] | |
| Ag clusters | Ag NCs/GC | 0.1 M KOH | 0.84 | / | / | / | 0.7 | [64] | |
| Ag NCs | 0.1 M KOH | 0.9 | 0.77 | 3.5 | 1600 | 3.47 | 0.5–2 | [65] | |
| Ag NC/CNs | 0.1 M KOH | 0.9 | / | 4.8 | 1600 | / | 2.88 ± 0.95 | [66] | |
| Ag NCs | 0.1 M KOH | 0.87 | 0.72 | / | / | / | 2 | [67] | |
| Pd clusters | Pd/C cubes | 0.1 M HClO ₄ | 0.98 | 0.87 | 5.8 | / | / | 3–5 | [68] |
| Pd/C Ligand off | 0.1 M KOH | 0.95 | 0.79 | 4.8 | 1600 | 3.9 | 1 | [69] | |
| Pd/CNs-20% | 0.1 M KOH | 0.96 | 0.82 | 5 | 1600 | 3.86–3.98 | 1.55 ± 0.55 | [70] | |
| Ru NG-750 | 0.1 M KOH | 0.9 | 0.83 | 2.9 | 900 | 4 | 5.8 ± 1.5 | [71] | |
| Ru cluster | 8(Pt-Ru) _{Cu} /GC | 0.1 M HClO ₄ | 0.95 | / | / | / | / | [72] | |
| Alloyed clusters | Au ₆₇ Pd ₃₃ /CNs | 0.1 M KOH | 0.94 | 0.83 | 5 | 2500 | 3.92–3.99 | 2.6 ± 0.8 | [73] |
| Pd modified GNCs | 0.1 M KOH | 0.97 | 0.84 | 4.8 | 2000 | 4 | 5 | [74] | |
| SL Pt ₃ Rh | 0.5 M H ₂ SO ₄ | 0.78 | 0.6 | 3.5 | 2400 | / | 3.3 ± 0.74 | [75] | |
| PtAu PNCs | 0.1 M KOH | 0.953 | 0.84 | 5.8 | 1600 | 3.62–3.87 | 3–6 | [76] | |

Pt₁₂@3: 12—the number of platinum atoms in the cluster, 3—the dendrimer generation number; G6-OH: the six generation dendrimer tailed by hydroxyl groups; DENs: dendrimer-encapsulated nanoparticles; Pt-3Sn: a Pt: Sn ratio of 1:3; GC: glassy carbon; OMPc: ordered mesoporous porphyrinic carbon; rGO: reduced graphene oxide; PyPBI: poly[2,2'-(pyridine-2,6-diyl)biphenimidazole-5,5'-diyl]; BOD-AuNC/SWNT: BOD-bilirubin oxidase, AuNCs—gold nanoclusters, SWNT—single walled carbon nanotubes; AuPC-1: PC-porous carbon, 1—the first sample; CNs—carbon nanosheets; NG—nitrogen-doped graphene; GNCs—gold nanoclusters; SL—supportless; PNCs—porous nanoclusters oxide.

3.1. Pt Clusters for ORR

Previous investigations have illustrated that Pt nanoparticles with a size ranging from a few to hundreds of nanometers are normally generated by the conventional synthetic approaches. To obtain Pt clusters, the macromolecule template such as dendrimer plays an essential role. Seminal and pioneering work has been conducted by Crooks' group, who prepared a series of dendrimer encapsulated Pt nanoclusters. In 2005, his group fabricated Pt nanoclusters of 1.4 nm in diameter embedded within fourth-generation, hydroxyl-terminated, poly(amidoamine) dendrimer for oxygen electrocatalytic reduction, and the resulting films can survive up to 50 consecutive cyclic voltammetric scans [77]. Subsequently, the size effects of Pt dendrimer-encapsulated nanoparticles on the kinetics toward ORR has also been probed by his group. Interestingly, with a series of Pt nanoparticles containing an average of 55, 100, 147, 200 and 240 Pt atoms, they found that the largest particles exhibited the highest specific activities [47]. In a following research effort, the effect of mass transfer on ORR catalyzed by Pt₅₅ and Pt₁₄₇ dendrimer encapsulated particles was also investigated by them [48].

In 2009, by using a phenylazomethine dendrimer, Yamamoto et al. successfully prepared a series of platinum clusters with a defined number of atoms [46]. The ORR activity of the Pt₁₂@3, Pt₂₈@3 and Pt₆₀@3 (3 = phenylazomethine) clusters is shown in Table 2. The highest catalytic performance was achieved for the smallest clusters, with a catalytic current approximately 13-times higher than that of commercially available Pt/C catalyst. Such performance variation between the Pt nanoparticles and ultra-small Pt clusters was further verified by Angelopoulos' group, who observed mass activities of about 48 A/g for the single crystals and 74 A/g for the atomic clusters with less than 20 Pt atoms [49].

Table 2. Comparison of cluster properties and the specific catalytic activity data for Ptn@3 ($n = 12$, 28 or 60) and Pt/C (TEC10E50E \#). Reproduced with permission [46]. Copyright 2009, the Nature Publishing Group.

| Catalyst | $N^* (N_{\text{surf}}^{\dagger})$ | Particle Size (nm) | $j_k/W_{\text{Pt}} (\mu\text{A cm}^{-2} \text{ng}_{\text{Pt}}^{-1})^{\ddagger}$ |
|---------------------|-----------------------------------|--------------------|---|
| Pt ₁₂ @3 | 12 (12) | 0.9 ± 0.1 | 46 ± 4 |
| Pt ₂₈ @3 | 28 (24) | 1.0 ± 0.1 | 23 ± 3 |
| Pt ₆₀ @3 | 60 (46) | 1.2 ± 0.1 | 18 ± 2 |
| Pt/C (TEC10E50E) | ~300 | 2.5 ± 0.5 | 3.6 ± 0.2 |

\# It's the product name. TEC: Product category name; 10: Alloy category, such as Pt, PtRu, PtCo; E: Carbon type; 50: Pt Loading percentage; E: Treatment type. $*$ Total number of platinum atoms in one cluster. † Number of platinum atoms appearing at the surface of the cluster. The cluster model was constructed to minimize the number of surface atoms based on face-centered cubic packing. ‡ Specific kinetic current density.

In 2013, a particle proximity effect for ORR was discovered by Arenz's group [78]. In this study, three different Pt nanocluster sizes were investigated, and the specific activity (SA) and mass activity are presented in Figure 1a,b. Surprisingly, no apparent correlation between the SA and nanocluster size is observed, and Pt_{>46}, but not Pt₂₀, exhibits the highest activity. This is because even Pt₂₀ is extremely small, so the number of adsorption sites is relatively low [78]. Figure 1c shows that the measured SA value depends on the edge-to-edge distance. When the average edge-to-edge distance diminishes below 1 nm, the SA of the various samples increased significantly, regardless of the Pt nanocluster size. That is, when the edge-to-edge interparticle distance is sufficiently small, ORR activities approaching the bulk Pt surface can be achieved for Pt clusters (Pt_{>46}). As a result, mass activity on Pt clusters up to six-times that of Pt/C catalysts was obtained [78]. Interestingly, such performance variation is also reflected in the change of the reaction mechanism, which can be experimentally extrapolated from the Tafel plots. The Tafel slope changed from 120 mV dec⁻¹ for the Pt crystals to 220 mV dec⁻¹ for the Pt clusters at high current density. Toyoda et al. found that the catalytic activity is actually correlated with the *d*-band center of the Pt nanoclusters. With the decreasing of cluster size, the *d*-band center moves forward to the Fermi level, which enhances the oxygen adsorption energy (stronger oxygen chemisorption) [50]. The first-principle calculations indicate that the enhancement was attributed to the electronic effects and geometric effects.

In addition to being directly applied as catalysts for ORR, Pt clusters can serve as modifiers or enhancers to promote the ORR activity. Note that coupling Pt with cost-effective and widely-available carbon materials can not only significantly improve the activity, but also lower the costs substantially. For instance, Vaarmets et al. prepared Pt-nanocluster-activated molybdenum carbide-derived carbon electrodes for oxygen electroreduction in 0.5 M H₂SO₄ [51]. The influence of specific surface area and microporosity-mesoporosity of Pt-nanocluster-modified carbide-derived carbon toward ORR was examined by Lust and coworkers [52]. In another study, Pt nanoclusters were decorated and highly distributed on Pd nanorods, and the Pt-on-Pd catalysts displayed a mass activity as high as 105.3 mA mg⁻¹ at 0.9 V with a Pt content as low as 1.5 wt% [53]. Park's group casted a trace amount of Pt nanoclusters on N-doped mesoporous porphyrinic carbon (OMPC) to enhance the intrinsic ORR activity, and 5 wt% Pt/FeCo-OMPC electrocatalyst was discovered to possess a factor of two improvement in mass activity compared to Pt/C [54].

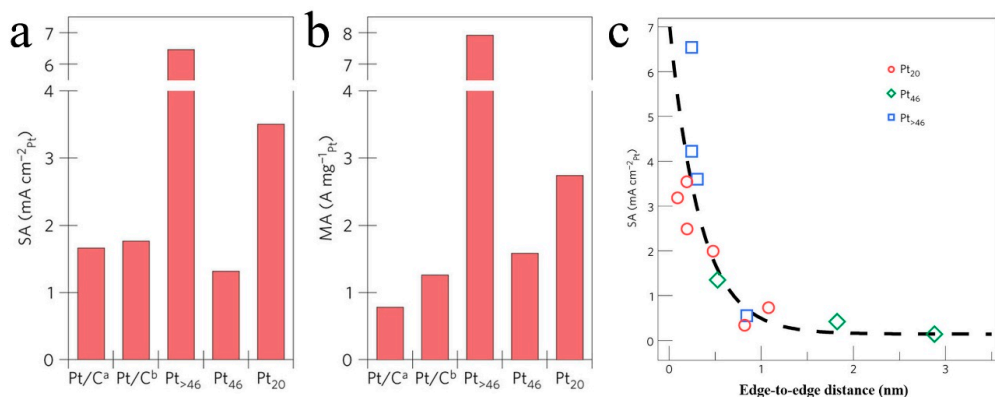


Figure 1. Specific activities (SAs) (a) and mass specific activities (MASes) (b) at 0.85 V_{RHE} for different Pt nanocluster samples. For comparison, the activities of two standard high-surface-area carbon-supported Pt catalysts (TKK, Tanda Kikinzoku Kogyo) are included, as well. Both standard catalysts have a Pt loading of 50 wt%; sample Pt/C^a has an average particle size of 5 nm, whereas the average particle size of sample Pt/C^b is 3 nm. (c) Specific activity versus edge-to-edge distance. The dashed line serves as a guide for the eye to highlight the observed trend. The measurements are performed at room temperature in 0.1 M HClO₄ electrolyte. Reproduced with permission [78]. Copyright 2013, the Nature Publishing Group.

It is worth mentioning that theoretical calculations also advanced the understanding of fundamental problems and underlying mechanisms in this aspect. The ORR activity of truncated octahedral Pt₃₈ clusters as a catalyst was investigated via first-principles simulations by Fortunelli's group. For Pt₃₈ clusters, the rate-determining step is the H₂O formation, while for an extended surface such as the Pt (111) crystal plane, the O hydration is actually the overall reaction barrier [79]. Recently, Nigam et al. carried out density function theory (DFT) calculations to examine the viability of alumina-supported Pt clusters (Pt_n@Al₂O₃, n = 1–7, 10) as ORR electrocatalysts [80]. It was found that the oxygen chemisorption on the alumina-supported Pt clusters is slightly weaker with elongated Pt-O bonds and ~8–10% lower reaction enthalpy compared with free Pt clusters.

3.2. Au Clusters for ORR

Bulk Au has attracted little attention in electrocatalysis, largely because of its poor catalytic performance. However, when it reaches nanoscale dimensions, the physicochemical properties of nanostructured Au exhibit a significant variation. Nanometer-sized Au nanoparticles especially Au clusters have been found to possess unusual catalytic activities toward a variety of reactions, such as CO oxidation [81], selective oxidation of styrene [31], aerobic oxidation of alcohol [82], selective hydrogenation of unsaturated ketones and aldehyde [83], as well as other reactions. Compared to their counterparts of gold nanocrystals or nanoparticles, the enhanced catalytic activity of Au nanoclusters is probably due to the high fraction of surface atoms with low coordination numbers. As the dimension decreases, such a fraction increases, featuring the advantages of employing Au clusters as catalysts.

Despite these progresses achieved regarding Au clusters for organic catalytic processes, Au clusters as electrocatalysts for ORR have not been paid attention to for quite a long time. Seminal work was done by Adzic's group, who found that the Pt ORR catalysts can be stabilized against dissolution under potential cycling regimes by modifying Pt nanoparticles with Au clusters [56]. In 2009, Chen et al. prepared a series of Au nanoclusters with 11–140 gold atoms in the cores and carried out detailed electrochemical studies in alkaline media to evaluate the size effect on the electrocatalytic activity in oxygen reduction [55]. The detailed structures of Au11, Au25, Au55 and Au144 clusters were elucidated and confirmed by MALDI-TOF (matrix-assisted laser desorption ionization-time of flight) analysis. The cyclic voltammograms and rotating disk electrode (RDE) voltammograms are presented in Figure 2. Figure 2a shows that the overall limiting current density (e.g., at –1.0 V) increases with

decreasing particle core size: Au_{11}/GC (-11.2 mA cm^{-2}) $>$ Au_{25}/GC (-10.1 mA cm^{-2}) $>$ Au_{55}/GC (-10.4 mA cm^{-2}) $>$ $\text{Au}_{140}/\text{GC}$ (-4.2 mA cm^{-2}), while Figure 2b illustrates that the onset potential of oxygen reduction shifts negatively: Au_{11}/GC (-0.10 V) $>$ Au_{25}/GC (-0.16 V) $>$ Au_{55}/GC (-0.20 V) $>$ $\text{Au}_{140}/\text{GC}$ (-0.25 V). One can conclude that a strong core-size effect was observed, and as the size decreased, the ORR activity increased [55]. This is due to the larger fraction of surface Au atoms with low coordination numbers in small-sized clusters. Meanwhile, with the decreasing of cluster size, the d -bands become narrowed and move toward the Fermi level [57,84], which is favorable for oxygen adsorption. Subsequently, molecule-like atomic Au₅ clusters were fabricated through a cetyltrimethylammonium bromide (CTAB)-assisted electrodeposition method by Phani's group, and a direct four-electron transfer pathway was observed in acid solution for these Au₅ clusters [85]. Interestingly, during the ORR catalytic process, a transition from a four-electron to a two-electron reduction was also shown, reflecting the transformation of Au clusters to Au nanoparticles. In 2012, Yin and Tang developed a novel and clean strategy to grow ultrafine Au clusters on reduced graphene oxide (RGO) nanosheets for electrochemical reduction of oxygen [58]. Recently, Fujigaya et al. described the growth and deposition of Au nanoclusters (diameter = 1.6 nm) on polymer-wrapped graphene, and an onset potential of -0.09 V (vs. AgCl/Ag) was achieved [59]. Another important recent contribution was made by Atanassov and Martinez' group, who prepared DNA templated Au nanoclusters of ~ 7 Au atoms as an enhancer of electron transfer and lowered the overpotential of ORR by $\sim 150 \text{ mV}$ compared to enzyme alone [60].

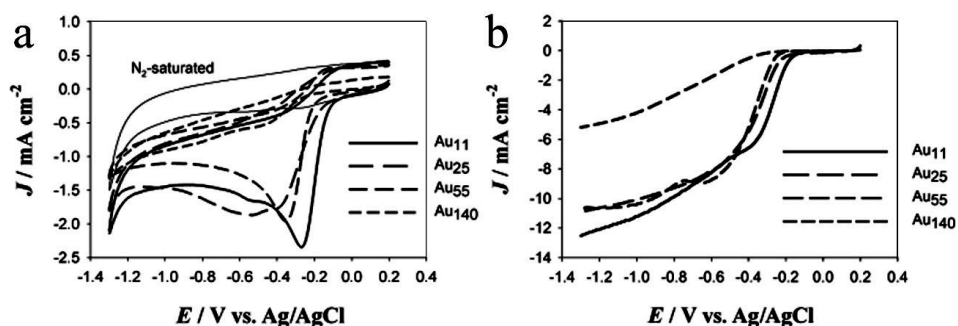


Figure 2. (a) Cyclic voltammograms of the Au_x/GC electrodes ($x = 11, 25, 55$ and 140) in 0.1 M KOH saturated with oxygen and of the Au_{11}/GC electrode in N_2 -saturated 0.1 M KOH solution (thin solid curve). Current density was calculated by normalizing the voltammetric currents to the effective Au active surface areas. Potential scan rate 0.1 V s^{-1} . (b) RDE voltammograms of varied Au_x/GC electrodes in 0.1 M KOH aqueous solution saturated by oxygen. Rotation rate 3600 rpm . Reproduced with permission [55]. Copyright 2009, Wiley-VCH.

Recently, our group has also conducted some work regarding employing Au clusters based nanocomposite for ORR. We integrated polyvinyl pyrrolidone (PVP)-protected Au nanoclusters with reduced graphene oxide (RGO) as the catalyst [61] and found that the nanocomposite possessed markedly higher long-term stability in ORR than Pt/C. Subsequently, we fabricated nanocomposite based on *p*-mercaptopbenzoic acid-functionalized Au nanoclusters, $\text{Au}_{102}(p\text{-MBA})_{44}$, and porous carbon nanosheets [62]. The best sample in the series composite exhibited slightly positive onset potential, but much higher long-term durability than Pt/C. We also synthesized a series of molecular Au clusters of $\text{Au}_{25}(\text{SC}_2\text{H}_4\text{Ph})_{18}$, $\text{Au}_{38}(\text{SC}_2\text{H}_4\text{Ph})_{24}$ and $\text{Au}_{144}(\text{SC}_2\text{H}_4\text{Ph})_{60}$ and employed them as precursors to porous carbon-supported Au nanoparticles with different sizes toward oxygen reduction [63]. The ORR performances of $\text{Au}_{25}(\text{SC}_2\text{H}_4\text{Ph})_{18}$, $\text{Au}_{38}(\text{SC}_2\text{H}_4\text{Ph})_{24}$, $\text{Au}_{144}(\text{SC}_2\text{H}_4\text{Ph})_{60}$ and the resulting AuPC-1, AuPC-2 and AuPC-3 samples are summarized in Table 3. One can see that, due to restraint of the surface thiolate ligand, the three molecular Au clusters exhibited relatively low ORR activity with $\text{Au}_{25}(\text{SC}_2\text{H}_4\text{Ph})_{18}$ being the best. However, upon the calcination and integration with porous carbon, significant enhancement can be observed. The optimal performance arose from

the smallest $\text{Au}_{25}(\text{SC}_2\text{H}_4\text{Ph})_{18}$ cluster-derived AuPC-1 sample, corresponding well with the previously well-established size effects [55]. Its ORR activity was also close to that of Pt/C, evidenced by comparable specific activity and more robust durability in chronoamperometric measurements [63].

Table 3. Comparison of the oxygen reduction reaction (ORR) activity of different samples calculated by voltammetric measurements in 0.1 M KOH solution. Reproduced with permission [63]. Copyright 2016, the American Chemical Society.

| Sample | E_p (V) ^a | j_p (mA cm^{-2}) ^a | E_{onset} (V) ^b | $E_{1/2}$ (V) ^b | j (mA cm^{-2} at +0.45 V ^b) | ECSA ($\text{m}^2 \text{g}^{-1}$) | Specific Activity at +0.80 V (mA cm^{-2}) | Mass Activity at +0.80 V (A g^{-1}) |
|--|------------------------|--|-------------------------------------|----------------------------|---|-------------------------------------|--|--|
| AuPC-1 | +0.86 | 0.45 | +0.95 | +0.83 | 3.61 | 32.02 | 0.612 | 25.50 |
| AuPC-2 | +0.83 | 0.36 | +0.91 | +0.78 | 3.21 | 30.13 | 0.195 | 8.13 |
| AuPC-3 | +0.80 | 0.33 | +0.89 | +0.75 | 3.16 | 27.27 | 0.160 | 6.67 |
| $\text{Au}_{25}(\text{SC}_2\text{H}_4\text{Ph})_{18}$ | +0.54 | 0.19 | +0.72 | +0.57 | 0.63 | | | |
| $\text{Au}_{38}(\text{SC}_2\text{H}_4\text{Ph})_{24}$ | +0.54 | 0.14 | +0.71 | +0.56 | 0.61 | | | |
| $\text{Au}_{144}(\text{SC}_2\text{H}_4\text{Ph})_{60}$ | +0.50 | 0.10 | +0.65 | +0.54 | 0.35 | | | |
| commercial Pt/C | +0.81 | 0.57 | +0.95 | +0.81 | 4.98 | 43.05 | 0.615 | 38.44 |

^a E_p and j_p were determined from cyclic voltammograms. ^b E_{onset} , $E_{1/2}$ and j at 0.45 V were determined from rotating disk voltammograms with a rotation speed of 2500 rpm. ECSA (electrochemical surface area) were determined from the cyclic voltammograms in 0.1 M N_2 -saturated HClO_4 solution.

3.3. Ag Clusters for ORR

Unlike Au nanoparticles or nanoclusters, earlier studies showed that the average electron transfer number is between two and four in ORR for Ag nanomaterials [86], suggesting that the final products include HO_2^- and OH^- . However, strong size effects toward ORR can be also observed for Ag nanomaterials. Lu and Chen prepared Ag nanoparticles with a diameter of 3.3 nm and Ag nanoclusters with a diameter of 0.7 nm and investigated their ORR performance in alkaline electrolyte [64]. Cyclic voltammetric measurements demonstrated that the onset potential was 150 mV more positive for 0.7 nm Ag nanoclusters than 3.3 nm Ag nanoparticles. Remarkably, compared to 3.3-nm Ag nanoparticles, the current density of ORR at −0.80 V was five-times higher than 3.3-nm Ag nanoparticles. However, for the 0.7-nm Ag nanoclusters, the ORR catalytic process is dominated first by a two-electron transfer pathway to produce H_2O_2 , and then, peroxide is further reduced by another two electrons to form water. The results deliver the message that Ag clusters might not be good ORR catalysts; however, when the clusters are even smaller and consist of only a few Ag atoms, the catalytic performance was significantly boosted. Yang et al. developed a high-yield strategy to synthesize very small Ag clusters with only 2–5 silver atoms [65], whose molecular structure and composition were revealed by MALDI-TOF analysis. The ORR activity of the Ag clusters, as well as citrate and 2-mercaptopbenzothiazole (MB)-protected Ag NPs is presented in Figure 3. From Figure 3a,b, both citrate and MB-protected Ag NPs barely exhibited ORR activity, while superior activity to commercial Pt/C from Ag clusters was acquired, evidenced by the more positive onset potential and larger kinetic current. Furthermore, as shown in Figure 3c, the measured H_2O_2 yield was below 15% for Ag clusters, comparable with that of Pt/C, but much slower than citrate and MB-protected Ag nanoparticles. The durability of the four samples was evaluated by chronoamperometric response (Figure 3d), which showed that Ag clusters exhibited a high current retention of 93% after 10,000 s, higher than citrate and MB-protected Ag nanoparticles, as well as Pt/C.

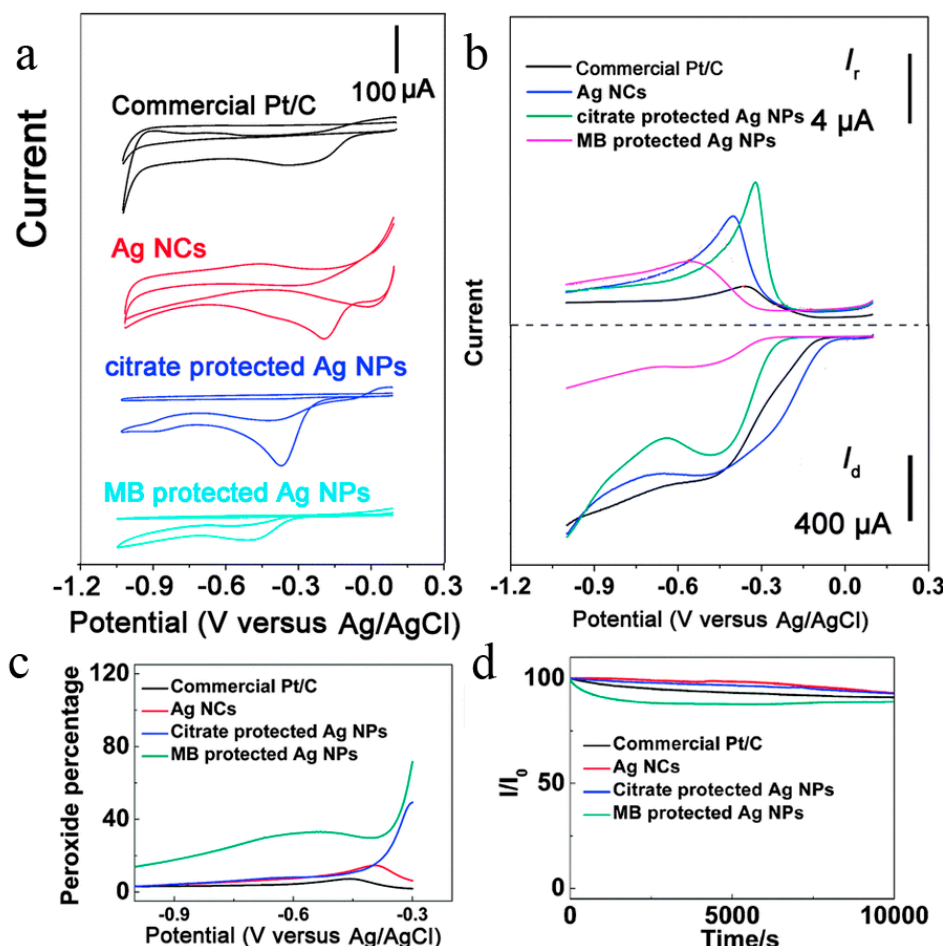


Figure 3. Ag nanoclusters as oxygen reduction catalysts. **(a)** CV curves of commercial Pt/C, Ag nanoclusters, citrate-protected Ag nanoparticles and 2-mercaptopbenzothiazole (MB)-protected Ag nanoparticles. **(b)** Rotating ring-disk electrode voltammograms recorded with different catalysts (loading: 0.1 mg cm^{-2}) in O_2 -saturated 0.1 M KOH at 1600 rpm . Disk current (I_d) (solid) is shown on the lower half, and ring current (I_r) is shown on the upper half of the graph. The disk potential was scanned at 10 mV s^{-1} , and the ring potential was constant at 0.5 V versus Ag/AgCl. **(c)** Percentage of peroxide of different catalysts at various potentials, based on the corresponding rotating ring-disk electron data in **(b)**. **(d)** Chronoamperometric responses for ORR of different catalysts in O_2 -saturated 0.1 M KOH at -0.3 V versus Ag/AgCl, respectively. Rotation rate: 200 rpm . Reproduced with permission [65]. Copyright 2014, Royal Society of Chemistry.

Besides directly using Ag clusters as catalysts for ORR, the carbon substrate can be introduced to integrate Ag clusters to enhance the electrocatalytic reduction of oxygen. Liu and Chen prepared “surfactant free” Ag clusters *in situ* supported on carbon nanodots, and the most efficient four-electron transfer process in ORR was observed [66]. Dong and Zhang’s group electrochemically-deposited Ag clusters on nitrogen-doped graphene, and such composite catalysts displayed comparable ORR performance with Pt/C, but enhanced methanol tolerance compared to Pt/C in alkaline solution [67]. Another interesting work was done by Clausmeyer and coworkers, who electrodeposited Ag clusters on bi-functional Θ-shaped nanoelectrodes for oxygen reduction. The high current densities observed for the ORR in chlor-alkali electrolyzers can be explained by the local oversaturation of O_2 in the direct vicinity of microscopic gas channels [87].

3.4. Pd and Ru Clusters for ORR

The continuous advancements of using Pt, Au and Ag clusters for oxygen electrocatalytic reduction have been inspiring the further endeavors of employing other noble metal clusters as ORR catalysts. Pd-based nanomaterials have been proven to be ORR active, as Pd can adsorb oxygen molecules and form stable and compact oxides [68]. Pd₁₃₋₁₇(SR)₁₈₋₂₂ clusters protected by 4-tert-butylbenzenethiolate have been successfully fabricated by Zhang and Jin's group [69]. Distinct ORR performance was observed for the ligand-on and ligand-off Pd clusters. Figure 4a shows that ligand-off Pd clusters exhibited a much sharper reduction peak, while from Figure 4b, more positive onset potential and larger diffusion-limited current from ligand-off Pd clusters than ligand-on clusters can be observed. Figure 4c shows that the mass activity of ligand-off Pd clusters is 272.4 A g⁻¹, about five-times that of ligand-on clusters, also much higher than that of Pt/C (166.66 A g⁻¹). The Tafel slopes calculated from Tafel plots (Figure 4d) for ligand-on and ligand-off clusters are -72.3 mV dec⁻¹ and -68.4 mV dec⁻¹, close to that value of Pt/C (~-60 mV dec⁻¹). Owing to the ligand protection, after 1000 cycles, no noticeable changes on onset potential and half-wave potential can be observed for the ligand on Pd clusters (Figure 4e), while a 10-mV decrease of half-wave potential was observed for the ligand off clusters (Figure 4f).

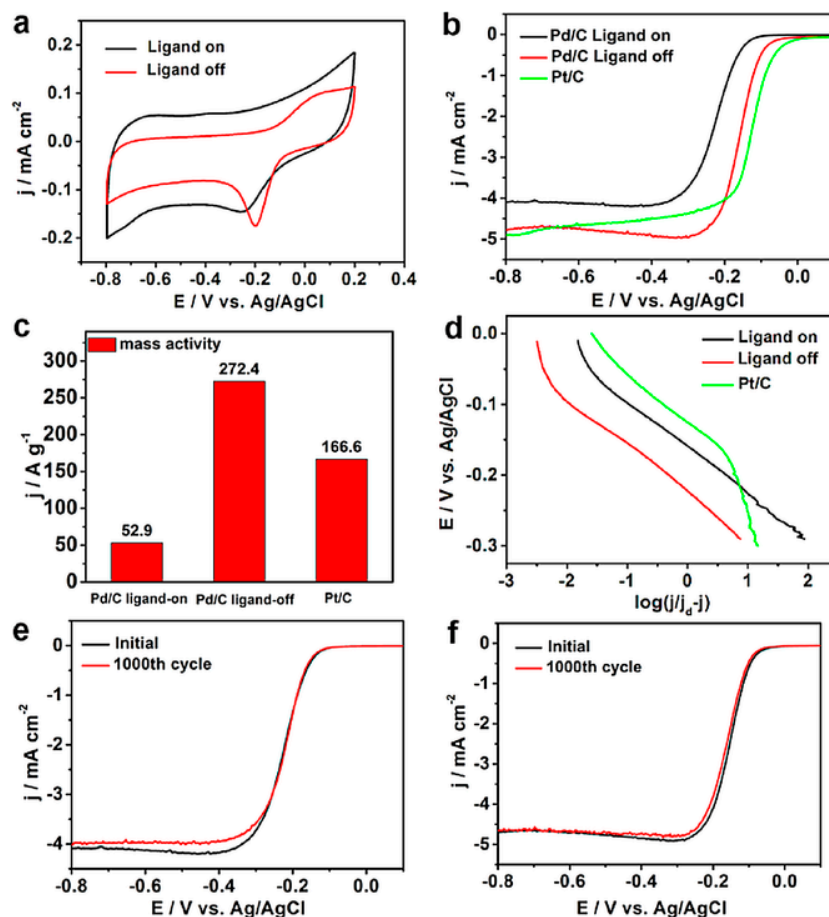


Figure 4. Electrochemical activities of ligand-on, ligand-off Pd_n/C and commercial Pt/C catalysts. (a) CV curves for ligand-on and ligand-off Pd_n/C catalysts in N₂-saturated 0.1 M KOH solutions; (b) ORR polarization curves for three catalysts in O₂-saturated 0.1 M KOH solutions at 1600 rpm; (c) mass activities for three catalysts at -0.15 V (vs. Ag/AgCl); (d) corresponding Tafel plots of ligand-on and ligand-off Pd_n/C catalysts and Pt/C catalysts ($\omega = 1600$ rpm); durability tests for ligand-on (e) and ligand-off (f) Pd_n/C nanocluster catalysts, respectively. All of the current densities are normalized to the geometric area of GC. Reproduced with permission [69]. Copyright 2016, Wiley-VCH.

Encouraged by these findings, our group prepared Pd clusters *in situ* encapsulated in porous carbon nanosheets (CNS) for ORR in alkaline media [70]. Electrochemical tests showed that Pd/CNS-20% (Pd mass loading is 20%) displayed superior activity than Pd black, with mass activity five-times greater than Pd black [70].

As a noble metal, Ru is much cheaper than Au, Ag, Pd and Pt. In a very recent study, Tour's group described the fabrication of Ru clusters supported on nitrogen-doped porous graphene (Ru/NG) as high-performance multifunctional electrocatalysts for ORR and hydrogen evolution reaction (HER), displaying similar activities to that of Pt/C in alkaline media [71]. Ru/NG can efficiently convert O₂ into OH⁻ in a four-electron pathway, showing great promise as an excellent candidate for cathode materials of fuel cells.

3.5. Alloyed Noble Metal Clusters for ORR

Till now, several studies have been documented regarding using alloyed bi-metallic noble metal clusters for ORR. The advantages of using alloys in the catalytic and electrocatalytic regime outperforming single metals can be summarized by the following factors. The marriage of two metals can endorse both a geometric effect and an electronic effect. The geometric effect refers to the generation of a new catalytic active site due to the combination of two metals [88]. The electronic structure can be altered due to the formation of the hetero-metal-metal bond, which can be favorable for catalytic reaction [88]. Furthermore, specifically for ORR, the combination of two metals can tune the adsorption capability of oxygen molecules. For example, both Pt and Pd possess strong binding affinity to oxygenated intermediates, while Au has little interaction with them, making both AuPt and AuPd optimal candidates for preparing binary alloys.

In 2009, Cukrowski's group reported for the first-time the fabrication of electrodeposited multilayer Ru-Pt clusters on glassy carbon for ORR in alkaline solution [72]. Yancey et al. electrochemically synthesized Au@Pt dendrimer-encapsulated nanoparticles and discovered that Au₁₄₇@Pt DENs (dendrimer encapsulated nanoparticles) exhibited higher ORR activity than Au and Pt nanoparticles alone [89].

By constructing multilayers of bare and Pd-modified Au clusters, Harada et al. also conducted electrocatalytic tests for ORR and found a significant increase in ORR rate after Pd deposition [74]. By using formic acid as the reducing agent, Balaji's group showcased the fabrication of self-stabilized Pt-Rh clusters toward ORR in sulfuric acid media [75]. The highest performance was achieved by the clusters with an optimal Pt-to-Rh ratio equaling 76.9:23.0, which adopted a four-electron pathway and retained 85% of its limiting current after 15,000 cycles of potential scans [75]. Recently, Feng and Xu developed a wet chemical approach to fabricate monodispersed porous dendrite-like PtAu porous nanoclusters for ORR and methanol oxidation by employing L-histidine as the structure-director and PVP as the dispersing agent [76]. In a recent report, our group described the preparation of AuPd clusters supported by porous carbon nanosheets in alkaline media [73]. In this study, a series of composites with different Au: Pd ratios (100:0, 80:20, 67:33, 50:50, 33:67, 20:80, 0:100) was prepared, and the electrocatalytic performance toward ORR is depicted in Figure 5. Figure 5a shows that the onset potential and diffusion limited current density varied drastically with the change of Au-to-Pd ratio, and the sample of Au₆₇Pd₃₃/CNS exhibited the best performance. Its ORR performance was then compared with Pt/C (Figure 5b), in which the onset potential of Au₆₇Pd₃₃/CNS (0.94 V) was close to that of Pt/C (0.96 V), while the diffusion-limited current density (5.13 mA cm⁻²) was higher than that of Pt/C (4.88 mA cm⁻²). The calculated electron transfer number and corresponding H₂O₂ yield can be found in Figure 5c. The Au₆₇Pd₃₃/CNS sample showed a high electron transfer number of 3.92–3.99 and a low H₂O₂ yield of less than 10% in the potential range of 0–+0.8 V, indicating that a direct four-electron transfer pathway was adopted with negligible byproduct produced. The reaction kinetics was then elucidated by extrapolating the Tafel slope from the Tafel plots (Figure 5d), and the Au₆₇Pd₃₃/CNS sample displayed a slope of 67.7 mV dec⁻¹, close to that of Pt/C (64.4 mV dec⁻¹). In addition, this sample also exhibited markedly superior long-term stability than that of Pt/C [73].

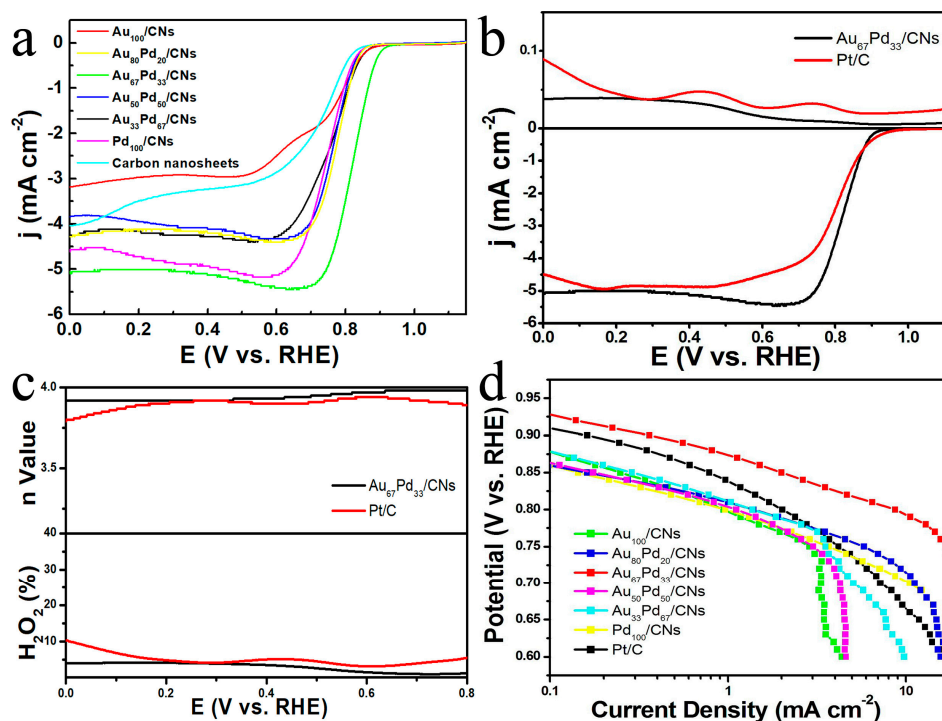


Figure 5. (a) Rotating ring-disk electrodes (RRDE) voltammograms of $\text{Au}_{100}/\text{CNs}$, $\text{Au}_{80}\text{Pd}_{20}/\text{CNs}$, $\text{Au}_{67}\text{Pd}_{33}/\text{CNs}$, $\text{Au}_{50}\text{Pd}_{50}/\text{CNs}$, $\text{Au}_{33}\text{Pd}_{67}/\text{CNs}$, $\text{Pd}_{100}/\text{CNs}$, and carbon nanosheets in O_2 -saturated 0.1 M KOH at 2500 rpm; (b) RRDE voltammograms; (c) plots of H_2O_2 yield and number of electrons transferred of a glassy carbon electrode modified with $\text{Au}_{67}\text{Pd}_{33}/\text{CNs}$ and commercial Pt/C catalyst; (d) the corresponding Tafel plots of $\text{Au}_{100}/\text{CNs}$, $\text{Au}_{80}\text{Pd}_{20}/\text{CNs}$, $\text{Au}_{67}\text{Pd}_{33}/\text{CNs}$, $\text{Au}_{50}\text{Pd}_{50}/\text{CNs}$, $\text{Au}_{33}\text{Pd}_{67}/\text{CNs}$, $\text{Pd}_{100}/\text{CNs}$ and commercial 20 wt% Pt/C. All measurements were tested with a catalyst loading of 80.8 mg cm^{-2} in an oxygen-saturated 0.1 M KOH aqueous solution at a potential scan rate of 10 mV s^{-1} . Reproduced with permission [73]. Copyright, Elsevier, 2017.

It is worth noting that these alloyed bimetallic clusters exhibited superior ORR performance than their counterparts of noble metal nanoparticles with larger sizes. For instance, with 0.1 M KOH as the electrolyte, the onset potential, half-wave potential and diffusion-limited current density at 1600 rpm were 0.95 V, 0.84 V and 5.8 mA cm^{-2} for PtAu porous nanocluster (size: ~3 nm), higher than for Pt@Au nanorods dispersed on pyridyne cycloaddition of graphene (size: ~20 nm in width, 0.89 V, 0.67 V and 5 mA cm^{-2}) [90]. Under almost the same conditions, the $\text{Au}_{67}\text{Pd}_{33}$ clusters supported on carbon nanosheets ($\text{Au}_{67}\text{Pd}_{33}/\text{CNs}$) [73] also exhibited more positive onset potential than AuPd alloy nanocrystals with reduced graphene oxide [91] (AuPd/rGO , size: 22.5 nm) (0.94 V for $\text{Au}_{67}\text{Pd}_{33}/\text{CNs}$ vs. 0.92 V for AuPd/rGO) and higher half-wave potential than reduced graphene oxide-supported asymmetric Au-core Pd-shell bimetallic nanoparticles [92] (Au@Pd/rGO , size: 15 nm) (0.83 V for $\text{Au}_{67}\text{Pd}_{33}/\text{CNs}$ vs. 0.80 V for Au@Pd/rGO). The above comparison further features the great advantages of employing metal clusters as highly efficient catalysts for ORR.

4. Challenges, Outlooks and Perspectives

Although great successes have been achieved using noble metal clusters for ORR, there are still several challenges and issues to be resolved. These problems include the shared challenges for all single metal clusters and alloyed clusters and specific issues for designated metal clusters. Challenges always mean opportunities, and further research efforts are encouraged to resolve these challenges, which actually form the outlook of this rapidly booming field.

One common issue is that the ligand served as the stabilizer to resist aggregation or enhance the longevity of the clusters in electrocatalytic process; however, the capping ligand also blocked some exposed active sites for the reaction. One way to mitigate this issue is to prepare ligand-free clusters or to directly encapsulate metal precursor in porous macromolecules then reduced by reductant to form metal clusters *in situ*. This is probably why we saw that more recent efforts are focusing on *in situ* methodologies, but further precise control of the monodispersity of metal clusters is urgently needed, which is one direction for future development. Another important common challenge might arise from the precise and accurate anchoring and integration of metal clusters with the support, which are insufficient in current investigations. To resolve this issue, rational design of the surface ligand structure and architecture, as well as the necessary modification of the support are essential, which are expected in future efforts. Lastly, how to further reduce the cost to match the market's expectation for large-scale commercialization of these noble metal clusters toward practical fuel cell application still has a long way to go.

In addition, there are also several specific challenges for different noble metal clusters and the alloyed clusters. For Pt and Au clusters, because of the ultra-high price, there is still necessity and room to further improve the intrinsic catalytic activity and cut the loadings of these two metals to reduce the costs. For Pd, Ag and Ru clusters, more precise atomic control of the nanocluster size is expected. Other noble metal clusters such as Rh and rare earth metals for ORR await to be explored. For alloyed clusters, besides the precise atomic control of the size, developing the criterion to fine-tune the optimized metallic ratio, but not by serendipitous discovery, is quite critical and worth more research endeavors. Theoretical calculation is certainly a powerful tool to advance the future development of this promising field.

Acknowledgments: Zhenghua Tang thanks the financial support from the National Natural Science Foundation of China (21501059), Guangdong Natural Science Funds for Distinguished Young Scholars (No. 2015A030306006), Guangdong Innovative and Entrepreneurial Research Team Program (No. 2014ZT05N200), as well as the Science and Technology Program of Guangdong Province (No. 2017A050506014).

Conflicts of Interest: The authors declare no conflict of interest.

References

1. Debe, M.K. Electrocatalyst approaches and challenges for automotive fuel cells. *Nature* **2012**, *486*, 43–51. [[CrossRef](#)] [[PubMed](#)]
2. Winter, M.; Brodd, R.J. What are batteries, fuel cells, and supercapacitors? *Chem. Rev.* **2004**, *104*, 4245–4270. [[CrossRef](#)] [[PubMed](#)]
3. Liu, M.; Zhang, R.; Chen, W. Graphene-supported nanoelectrocatalysts for fuel cells: Synthesis, properties, and applications. *Chem. Rev.* **2014**, *114*, 5117–5160. [[CrossRef](#)] [[PubMed](#)]
4. Wu, G.; Wang, J.; Ding, W.; Nie, Y.; Li, L.; Qi, X.; Chen, S.; Wei, Z. A strategy to promote the electrocatalytic activity of spinels for oxygen reduction by structure reversal. *Angew. Chem. Int. Ed.* **2016**, *55*, 1340–1344. [[CrossRef](#)] [[PubMed](#)]
5. Wu, G.; Santandreu, A.; Kellogg, W.; Gupta, S.; Ogoke, O.; Zhang, H.; Wang, H.-L.; Dai, L. Carbon nanocomposite catalysts for oxygen reduction and evolution reactions: From nitrogen doping to transition-metal addition. *Nano Energy* **2016**, *29*, 83–110. [[CrossRef](#)]
6. Shao, M.; Chang, Q.; Dodelet, J.-P.; Chenitz, R. Recent advances in electrocatalysts for oxygen reduction reaction. *Chem. Rev.* **2016**, *116*, 3594–3657. [[CrossRef](#)] [[PubMed](#)]
7. Huang, X.; Zhao, Z.; Cao, L.; Chen, Y.; Zhu, E.; Lin, Z.; Li, M.; Yan, A.; Zettl, A.; Wang, Y.M.; et al. High-performance transition metal-doped Pt₃Ni octahedra for oxygen reduction reaction. *Science* **2015**, *348*, 1230–1234. [[CrossRef](#)] [[PubMed](#)]
8. Bu, L.; Zhang, N.; Guo, S.; Zhang, X.; Li, J.; Yao, J.; Wu, T.; Lu, G.; Ma, J.-Y.; Su, D.; et al. Biaxially strained PtPb/Pt core/shell nanoplate boosts oxygen reduction catalysis. *Science* **2016**, *354*, 1410–1414. [[CrossRef](#)] [[PubMed](#)]

9. Wang, Y.-J.; Zhao, N.; Fang, B.; Li, H.; Bi, X.T.; Wang, H. Carbon-supported Pt-based alloy electrocatalysts for the oxygen reduction reaction in polymer electrolyte membrane fuel cells: Particle size, shape, and composition manipulation and their impact to activity. *Chem. Rev.* **2015**, *115*, 3433–3467. [CrossRef] [PubMed]
10. Wu, J.; Yang, H. Platinum-based oxygen reduction electrocatalysts. *Acc. Chem. Res.* **2013**, *46*, 1848–1857. [CrossRef] [PubMed]
11. Luo, M.; Guo, S. Strain-controlled electrocatalysis on multimetallic nanomaterials. *Nat. Rev. Mater.* **2017**, *2*, 17059. [CrossRef]
12. Lv, H.; Li, D.; Strmcnik, D.; Paulikas, A.P.; Markovic, N.M.; Stamenkovic, V.R. Recent advances in the design of tailored nanomaterials for efficient oxygen reduction reaction. *Nano Energy* **2016**, *29*, 149–165. [CrossRef]
13. Xia, W.; Mahmood, A.; Liang, Z.; Zou, R.; Guo, S. Earth-abundant nanomaterials for oxygen reduction. *Angew. Chem. Int. Ed.* **2016**, *55*, 2650–2676. [CrossRef] [PubMed]
14. Cui, C.-H.; Yu, S.-H. Engineering interface and surface of noble metal nanoparticle nanotubes toward enhanced catalytic activity for fuel cell applications. *Acc. Chem. Res.* **2013**, *46*, 1427–1437. [CrossRef] [PubMed]
15. Wang, Y.-J.; Wilkinson, D.P.; Zhang, J. Noncarbon support materials for polymer electrolyte membrane fuel cell electrocatalysts. *Chem. Rev.* **2011**, *111*, 7625–7651. [CrossRef] [PubMed]
16. Murray, R.W. Nanoelectrochemistry: Metal nanoparticles, nanoelectrodes, and nanopores. *Chem. Rev.* **2008**, *108*, 2688–2720. [CrossRef] [PubMed]
17. Wang, S.; Yu, H.; Zhu, M. Noble and valuable: Atomically precise gold nanoclusters. *Sci. China Chem.* **2016**, *59*, 206–208. [CrossRef]
18. Jin, R.; Zeng, C.; Zhou, M.; Chen, Y. Atomically precise colloidal metal nanoclusters and nanoparticles: Fundamentals and opportunities. *Chem. Rev.* **2016**, *116*, 10346–10413. [CrossRef] [PubMed]
19. Lu, Y.; Chen, W. Sub-nanometre sized metal clusters: From synthetic challenges to the unique property discoveries. *Chem. Soc. Rev.* **2012**, *41*, 3594–3623. [CrossRef] [PubMed]
20. Brust, M.; Walker, M.; Bethell, D.; Schiffrin, D.J.; Whyman, R. Synthesis of thiol-derivatized gold nanoparticles in a 2-phase liquid-liquid system. *J. Chem. Soc. Chem. Commun.* **1994**, 801–802. [CrossRef]
21. Brust, M.; Fink, J.; Bethell, D.; Schiffrin, D.J.; Kiely, C. Synthesis and reactions of functionalised gold nanoparticles. *J. Chem. Soc. Chem. Commun.* **1995**, 1655–1656. [CrossRef]
22. Li, G.; Jin, R. Atomically precise gold nanoclusters as new model catalysts. *Acc. Chem. Res.* **2013**, *46*, 1749–1758. [CrossRef] [PubMed]
23. Jin, R. Atomically precise metal nanoclusters: Stable sizes and optical properties. *Nanoscale* **2015**, *7*, 1549–1565. [CrossRef] [PubMed]
24. Zhu, M.; Lanni, E.; Garg, N.; Bier, M.E.; Jin, R. Kinetically controlled, high-yield synthesis of Au₂₅ clusters. *J. Am. Chem. Soc.* **2008**, *130*, 1138–1139. [CrossRef] [PubMed]
25. Qian, H.; Zhu, Y.; Jin, R. Size-focusing synthesis, optical and electrochemical properties of monodisperse Au(38)(SC(2)H(4)Ph)(24) nanoclusters. *ACS Nano* **2009**, *3*, 3795–3803. [CrossRef] [PubMed]
26. Tang, Z.; Xu, B.; Wu, B.; Germann, M.W.; Wang, G. Synthesis and structural determination of multidentate 2,3-dithiol-stabilized Au clusters. *J. Am. Chem. Soc.* **2010**, *132*, 3367–3374. [CrossRef] [PubMed]
27. McKenzie, L.C.; Zaikova, T.O.; Hutchison, J.E. Structurally similar triphenylphosphine-stabilized undecagolds, Au₁₁(PPh₃)₇Cl₃ and [Au₁₁(PPh₃)₈Cl₂]Cl, exhibit distinct ligand exchange pathways with glutathione. *J. Am. Chem. Soc.* **2014**, *136*, 13426–13435. [CrossRef] [PubMed]
28. Das, A.; Liu, C.; Byun, H.Y.; Nobusada, K.; Zhao, S.; Rosi, N.; Jin, R. Structure determination of [Au₁₈(SR)₁₄]. *Angew. Chem. Int. Ed.* **2015**, *54*, 3140–3144. [CrossRef] [PubMed]
29. Chen, S.; Wang, S.; Zhong, J.; Song, Y.; Zhang, J.; Sheng, H.; Pei, Y.; Zhu, M. The structure and optical properties of the [Au₁₈(SR)₁₄] nanocluster. *Angew. Chem. Int. Ed.* **2015**, *54*, 3145–3149. [CrossRef] [PubMed]
30. Parker, J.F.; Fields-Zinna, C.A.; Murray, R.W. The story of a monodisperse gold nanoparticle: Au₂₅L₁₈. *Acc. Chem. Res.* **2010**, *43*, 1289–1296. [CrossRef] [PubMed]
31. Turner, M.; Golovko, V.B.; Vaughan, O.P.H.; Abdulkhin, P.; Berenguer-Murcia, A.; Tikhov, M.S.; Johnson, B.F.G.; Lambert, R.M. Selective oxidation with dioxygen by gold nanoparticle catalysts derived from 55-atom clusters. *Nature* **2008**, *454*, 981–984. [CrossRef] [PubMed]

32. Levi-Kalisman, Y.; Jadzinsky, P.D.; Kalisman, N.; Tsunoyama, H.; Tsukuda, T.; Bushnell, D.A.; Kornberg, R.D. Synthesis and characterization of Au(102)(*p*-MBA)(44) nanoparticles. *J. Am. Chem. Soc.* **2011**, *133*, 2976–2982. [CrossRef] [PubMed]
33. Tang, Z.; Robinson, D.A.; Bokossa, N.; Xu, B.; Wang, S.; Wang, G. Mixed dithiolate durene-dt and monothiolate phenylethanethiolate protected Au130 nanoparticles with discrete core and core-ligand energy states. *J. Am. Chem. Soc.* **2011**, *133*, 16037–16044. [CrossRef] [PubMed]
34. Qian, H.; Jin, R. Controlling nanoparticles with atomic precision: The case of Au(144)(SCH(2)CH(2)Ph)(60). *Nano Lett.* **2009**, *9*, 4083–4087. [CrossRef] [PubMed]
35. Heaven, M.W.; Dass, A.; White, P.S.; Holt, K.M.; Murray, R.W. Crystal structure of the gold nanoparticle N(C₈H₁₇)₄ Au25(SCH₂CH₂Ph)₁₈. *J. Am. Chem. Soc.* **2008**, *130*, 3754–3755. [CrossRef] [PubMed]
36. Zhu, M.; Aikens, C.M.; Hollander, F.J.; Schatz, G.C.; Jin, R. Correlating the crystal structure of a thiol-protected Au25 cluster and optical properties. *J. Am. Chem. Soc.* **2008**, *130*, 5883–5885. [CrossRef] [PubMed]
37. Qian, H.; Eckenhoff, W.T.; Zhu, Y.; Pintauer, T.; Jin, R. Total structure determination of thiolate-protected Au(38) nanoparticles. *J. Am. Chem. Soc.* **2010**, *132*, 8280–8281. [CrossRef] [PubMed]
38. Jadzinsky, P.D.; Calero, G.; Ackerson, C.J.; Bushnell, D.A.; Kornberg, R.D. Structure of a thiol monolayer-protected gold nanoparticle at 1.1 Å resolution. *Science* **2007**, *318*, 430–432. [CrossRef] [PubMed]
39. Guo, S.; Zhang, S.; Sun, S. Tuning nanoparticle catalysis for the oxygen reduction reaction. *Angew. Chem. Int. Ed.* **2013**, *52*, 8526–8544. [CrossRef] [PubMed]
40. Wang, W.; Lei, B.; Guo, S. Engineering multimetallic nanocrystals for highly efficient oxygen reduction catalysts. *Adv. Energy Mater.* **2016**, *6*, 1600236. [CrossRef]
41. Jiao, Y.; Zheng, Y.; Jaroniec, M.; Qiao, S.Z. Design of electrocatalysts for oxygen- and hydrogen-involving energy conversion reactions. *Chem. Soc. Rev.* **2015**, *44*, 2060–2086. [CrossRef] [PubMed]
42. Yu, L.; Pan, X.; Cao, X.; Hu, P.; Bao, X. Oxygen reduction reaction mechanism on nitrogen-doped graphene: A density functional theory study. *J. Catal.* **2011**, *282*, 183–190. [CrossRef]
43. Nilekar, A.U.; Mavrikakis, M. Improved oxygen reduction reactivity of platinum monolayers on transition metal surfaces. *Surf. Sci.* **2008**, *602*, L89–L94. [CrossRef]
44. Nørskov, J.K.; Rossmeisl, J.; Logadottir, A.; Lindqvist, L.; Kitchin, J.R.; Bligaard, T.; Jónsson, H. Origin of the overpotential for oxygen reduction at a fuel-cell cathode. *J. Phys. Chem. B* **2004**, *108*, 17886–17892. [CrossRef]
45. Stephens, I.E.L.; Bondarenko, A.S.; Gronbjerg, U.; Rossmeisl, J.; Chorkendorff, I. Understanding the electrocatalysis of oxygen reduction on platinum and its alloys. *Energy Environ. Sci.* **2012**, *5*, 6744–6762. [CrossRef]
46. Yamamoto, K.; Imaoka, T.; Chun, W.-J.; Enoki, O.; Katoh, H.; Takenaga, M.; Sonoi, A. Size-specific catalytic activity of platinum clusters enhances oxygen reduction reactions. *Nat. Chem.* **2009**, *1*, 397–402. [CrossRef] [PubMed]
47. Ye, H.; Crooks, J.A.; Crooks, R.M. Effect of particle size on the kinetics of the electrocatalytic oxygen reduction reaction catalyzed by Pt dendrimer-encapsulated nanoparticles. *Langmuir* **2007**, *23*, 11901–11906. [CrossRef] [PubMed]
48. Dumitrescu, I.; Crooks, R.M. Effect of mass transfer on the oxygen reduction reaction catalyzed by platinum dendrimer encapsulated nanoparticles. *Proc. Nat. Acad. Sci. USA* **2012**, *109*, 11493–11497. [CrossRef] [PubMed]
49. St. John, S.; Dutta, I.; Angelopoulos, A.P. Synthesis and characterization of electrocatalytically active platinum atom clusters and monodisperse single crystals. *J. Phys. Chem. C* **2010**, *114*, 13515–13525. [CrossRef]
50. Toyoda, E.; Jinnouchi, R.; Hatanaka, T.; Morimoto, Y.; Mitsuhashi, K.; Visikovskiy, A.; Kido, Y. The d-band structure of Pt nanoclusters correlated with the catalytic activity for an oxygen reduction reaction. *J. Phys. Chem. C* **2011**, *115*, 21236–21240. [CrossRef]
51. Vaarmets, K.; Nerut, J.; Häärk, E.; Lust, E. Electrochemical and physical characterisation of Pt-nanocluster activated molybdenum carbide derived carbon electrodes. *Electrochim. Acta* **2013**, *104*, 216–227. [CrossRef]
52. Lust, E.; Vaarmets, K.; Nerut, J.; Tallo, I.; Valk, P.; Sepp, S.; Häärk, E. Influence of specific surface area and microporosity-mesoporosity of pristine and Pt-nanoclusters modified carbide derived carbon electrodes on the oxygen electroreduction. *Electrochim. Acta* **2014**, *140*, 294–303. [CrossRef]
53. Yang, T.; Cao, G.; Huang, Q.; Ma, Y.; Wan, S.; Zhao, H.; Li, N.; Sun, X.; Yin, F. Surface-limited synthesis of Pt nanocluster decorated pd hierarchical structures with enhanced electrocatalytic activity toward oxygen reduction reaction. *ACS Appl. Mater. Interfaces* **2015**, *7*, 17162–17170. [CrossRef] [PubMed]

54. Hwang, S.-M.; Choi, Y.; Kim, M.G.; Sohn, Y.-J.; Cheon, J.Y.; Joo, S.H.; Yim, S.-D.; Kuttiyiel, K.A.; Sasaki, K.; Adzic, R.R.; et al. Enhancement of oxygen reduction reaction activities by Pt nanoclusters decorated on ordered mesoporous porphyrinic carbons. *J. Mater. Chem. A* **2016**, *4*, 5869–5876. [CrossRef]
55. Chen, W.; Chen, S. Oxygen electroreduction catalyzed by gold nanoclusters: Strong core size effects. *Angew. Chem. Int. Ed.* **2009**, *48*, 4386–4389. [CrossRef] [PubMed]
56. Zhang, J.; Sasaki, K.; Sutter, E.; Adzic, R.R. Stabilization of platinum oxygen-reduction electrocatalysts using gold clusters. *Science* **2007**, *315*, 220–222. [CrossRef] [PubMed]
57. Tang, W.; Lin, H.; Kleiman-Shwarsctein, A.; Stucky, G.D.; McFarland, E.W. Size-dependent activity of gold nanoparticles for oxygen electroreduction in alkaline electrolyte. *J. Phys. Chem. C* **2008**, *112*, 10515–10519. [CrossRef]
58. Yin, H.; Tang, H.; Wang, D.; Gao, Y.; Tang, Z. Facile synthesis of surfactant-free Au cluster/graphene hybrids for high-performance oxygen reduction reaction. *ACS Nano* **2012**, *6*, 8288–8297. [CrossRef] [PubMed]
59. Fujigaya, T.; Kim, C.; Hamasaki, Y.; Nakashima, N. Growth and deposition of Au nanoclusters on polymer-wrapped graphene and their oxygen reduction activity. *Sci. Rep.* **2016**, *6*, 21314. [CrossRef] [PubMed]
60. Chakraborty, S.; Babanova, S.; Rocha, R.C.; Desiraju, A.; Artyushkova, K.; Boncella, A.E.; Atanassov, P.; Martinez, J.S. A hybrid DNA-templated gold nanocluster for enhanced enzymatic reduction of oxygen. *J. Am. Chem. Soc.* **2015**, *137*, 11678–11687. [CrossRef] [PubMed]
61. Wang, C.; Li, N.; Wang, Q.; Tang, Z. Hybrid nanomaterials based on graphene and gold nanoclusters for efficient electrocatalytic reduction of oxygen. *Nanoscale Res. Lett.* **2016**, *11*, 336. [CrossRef] [PubMed]
62. Wang, Q.; Wang, L.; Tang, Z.; Wang, F.; Yan, W.; Yang, H.; Zhou, W.; Li, L.; Kang, X.; Chen, S. Oxygen reduction catalyzed by gold nanoclusters supported on carbon nanosheets. *Nanoscale* **2016**, *8*, 6629–6635. [CrossRef] [PubMed]
63. Wang, L.; Tang, Z.; Yan, W.; Yang, H.; Wang, Q.; Chen, S. Porous carbon-supported gold nanoparticles for oxygen reduction reaction: Effects of nanoparticle size. *ACS Appl. Mater. Interfaces* **2016**, *8*, 20635–20641. [CrossRef] [PubMed]
64. Lu, Y.; Chen, W. Size effect of silver nanoclusters on their catalytic activity for oxygen electro-reduction. *J. Power Sources* **2012**, *197*, 107–110. [CrossRef]
65. Yang, X.; Gan, L.; Zhu, C.; Lou, B.; Han, L.; Wang, J.; Wang, E. A dramatic platform for oxygen reduction reaction based on silver nanoclusters. *Chem. Commun.* **2014**, *50*, 234–236. [CrossRef] [PubMed]
66. Liu, M.; Chen, W. Green synthesis of silver nanoclusters supported on carbon nanodots: Enhanced photoluminescence and high catalytic activity for oxygen reduction reaction. *Nanoscale* **2013**, *5*, 12558–12564. [CrossRef] [PubMed]
67. Jin, S.; Chen, M.; Dong, H.; He, B.; Lu, H.; Su, L.; Dai, W.; Zhang, Q.; Zhang, X. Stable silver nanoclusters electrochemically deposited on nitrogen-doped graphene as efficient electrocatalyst for oxygen reduction reaction. *J. Power Sources* **2015**, *274*, 1173–1179. [CrossRef]
68. Zhang, H.; Jin, M.; Xiong, Y.; Lim, B.; Xia, Y. Shape-controlled synthesis of Pd nanocrystals and their catalytic applications. *Acc. Chem. Res.* **2013**, *46*, 1783–1794. [CrossRef] [PubMed]
69. Zhao, S.; Zhang, H.; House, S.D.; Jin, R.; Yang, J.C.; Jin, R. Ultrasmall palladium nanoclusters as effective catalyst for oxygen reduction reaction. *ChemElectroChem* **2016**, *3*, 1225–1229. [CrossRef]
70. Yan, W.; Tang, Z.; Li, L.; Wang, L.; Yang, H.; Wang, Q.; Wu, W.; Chen, S. Ultrasmall palladium nanoclusters encapsulated in porous carbon nanosheets for oxygen electroreduction in alkaline media. *ChemElectroChem* **2017**, *4*, 1349–1355. [CrossRef]
71. Ye, R.; Liu, Y.; Peng, Z.; Wang, T.; Jalilov, A.S.; Yakobson, B.I.; Wei, S.-H.; Tour, J.M. High performance electrocatalytic reaction of hydrogen and oxygen on ruthenium nanoclusters. *ACS Appl. Mater. Interfaces* **2017**, *9*, 3785–3791. [CrossRef] [PubMed]
72. Mkwizu, T.S.; Mathe, M.K.; Cukrowski, I. Electrodeposition of multilayered bimetallic nanoclusters of ruthenium and platinum via surface-limited redox-replacement reactions for electrocatalytic applications. *Langmuir* **2010**, *26*, 570–580. [CrossRef] [PubMed]
73. Yan, W.; Tang, Z.; Wang, L.; Wang, Q.; Yang, H.; Chen, S. PdAu alloyed clusters supported by carbon nanosheets as efficient electrocatalysts for oxygen reduction. *Int. J. Hydrogen Energy* **2017**, *42*, 218–227. [CrossRef]

74. Motoko, H.; Hidenori, N.; Nikolas, Z.; Satoru, T.; Wenbo, S.; Kohei, U. Construction of multilayers of bare and pd modified gold nanoclusters and their electrocatalytic properties for oxygen reduction. *Sci. Technol. Adv. Mater.* **2011**, *12*, 044606.
75. Narayananamoorthy, B.; Datta, K.K.R.; Eswaramoorthy, M.; Balaji, S. Self-stabilized Pt-Rh bimetallic nanoclusters as durable electrocatalysts for dioxygen reduction in PEM fuel cells. *RSC Adv.* **2014**, *4*, 55571–55579. [CrossRef]
76. Xie, X.-W.; Lv, J.-J.; Liu, L.; Wang, A.-J.; Feng, J.-J.; Xu, Q.-Q. Amino acid-assisted fabrication of uniform dendrite-like PtAu porous nanoclusters as highly efficient electrocatalyst for methanol oxidation and oxygen reduction reactions. *Int. J. Hydrogen Energy* **2017**, *42*, 2104–2115. [CrossRef]
77. Ye, H.; Crooks, R.M. Electrocatalytic O₂ reduction at glassy carbon electrodes modified with dendrimer-encapsulated Pt nanoparticles. *J. Am. Chem. Soc.* **2005**, *127*, 4930–4934. [CrossRef] [PubMed]
78. Nesselberger, M.; Roefzaad, M.; Fayçal Hamou, R.; Ulrich Biedermann, P.; Schweinberger, F.F.; Kunz, S.; Schloegl, K.; Wiberg, G.K.H.; Ashton, S.; Heiz, U.; et al. The effect of particle proximity on the oxygen reduction rate of size-selected platinum clusters. *Nat. Mater.* **2013**, *12*, 919. [CrossRef] [PubMed]
79. Sementa, L.; Andreussi, O.; Goddard, W.A.; Fortunelli, A. Catalytic activity of Pt-38 in the oxygen reduction reaction from first-principles simulations. *Catal. Sci. Technol.* **2016**, *6*, 6901–6909. [CrossRef]
80. Nigam, S.; Majumder, C. Orr viability of alumina-supported platinum nanocluster: Exploring oxidation behaviour by DFT. *Phys. Chem. Chem. Phys.* **2017**, *19*, 19308–19315. [CrossRef] [PubMed]
81. Wu, Z.; Jiang, D.-E.; Mann, A.K.P.; Mullins, D.R.; Qiao, Z.-A.; Allard, L.F.; Zeng, C.; Jin, R.; Overbury, S.H. Thiolate ligands as a double-edged sword for CO oxidation on CeO₂ supported Au₂₅(SCH₂CH₂Ph)₁₈ nanoclusters. *J. Am. Chem. Soc.* **2014**, *136*, 6111–6122. [CrossRef] [PubMed]
82. Yamazoe, S.; Koyasu, K.; Tsukuda, T. Nonscalable oxidation catalysis of gold clusters. *Acc. Chem. Res.* **2013**, *47*, 816–824. [CrossRef] [PubMed]
83. Zhu, Y.; Qian, H.; Drake, B.A.; Jin, R. Atomically precise Au(25)(SR)(18) nanoparticles as catalysts for the selective hydrogenation of alpha,beta-unsaturated ketones and aldehydes. *Angew. Chem. Int. Ed.* **2010**, *49*, 1295–1298. [CrossRef] [PubMed]
84. van Bokhoven, J.A.; Miller, J.T. D electron density and reactivity of the d band as a function of particle size in supported gold catalysts. *J. Phys. Chem. C* **2007**, *111*, 9245–9249. [CrossRef]
85. Jeyabharathi, C.; Senthil Kumar, S.; Kiruthika, G.V.M.; Phani, K.L.N. Aqueous CTAB-assisted electrodeposition of gold atomic clusters and their oxygen reduction electrocatalytic activity in acid solutions. *Angew. Chem. Int. Ed.* **2010**, *49*, 2925–2928. [CrossRef] [PubMed]
86. Campbell, F.W.; Belding, S.R.; Baron, R.; Xiao, L.; Compton, R.G. Hydrogen peroxide electroreduction at a silver-nanoparticle array: Investigating nanoparticle size and coverage effects. *J. Phys. Chem. C* **2009**, *113*, 9053–9062. [CrossRef]
87. Clausmeyer, J.; Botz, A.; Ohl, D.; Schuhmann, W. The oxygen reduction reaction at the three-phase boundary: Nanoelectrodes modified with Ag nanoclusters. *Faraday Discuss.* **2016**, *193*, 241–250. [CrossRef] [PubMed]
88. Gilroy, K.D.; Ruditskiy, A.; Peng, H.-C.; Qin, D.; Xia, Y. Bimetallic nanocrystals: Syntheses, properties, and applications. *Chem. Rev.* **2016**, *116*, 10414–10472. [CrossRef] [PubMed]
89. Yancey, D.F.; Carino, E.V.; Crooks, R.M. Electrochemical synthesis and electrocatalytic properties of Au@Pt dendrimer-encapsulated nanoparticles. *J. Am. Chem. Soc.* **2010**, *132*, 10988–10989. [CrossRef] [PubMed]
90. Zhong, X.; Yu, H.; Wang, X.; Liu, L.; Jiang, Y.; Wang, L.; Zhuang, G.; Chu, Y.; Li, X.; Wang, J.-G. Pt@Au nanorods uniformly decorated on pyridyne cycloaddition graphene as a highly effective electrocatalyst for oxygen reduction. *ACS Appl. Mater. Interfaces* **2014**, *6*, 13448–13454. [CrossRef] [PubMed]
91. Lin, X.-X.; Zhang, X.-F.; Wang, A.-J.; Fang, K.-M.; Yuan, J.; Feng, J.-J. Simple one-pot aqueous synthesis of AuPd alloy nanocrystals/reduced graphene oxide as highly efficient and stable electrocatalyst for oxygen reduction and hydrogen evolution reactions. *J. Colloid Interface Sci.* **2017**, *499*, 128–137. [CrossRef] [PubMed]
92. Noh, S.; Shim, J.H. Asymmetric Au-core Pd-shell nanoparticles supported on reduced graphene oxide for enhanced electrocatalytic activity. *RSC Adv.* **2016**, *6*, 84334–84341. [CrossRef]

